Autonomous-synergic Voltage Security Regions in Bulk Power Systems

Fan Li, Tao Niu, Lin Xue, Yuxiao Li, Tianen Huang, and Zhenjie Wu

***Abstract*—Determining security/stability boundaries is a common and critical means of preventing cascading failures induced by voltage-related issues, which represents one of the major challenges in bulk power systems. However, traditional approaches suffer from conservative issues and heavy computational burdens. To address these challenges, the concept of an autonomous-synergic voltage security region (AS-VSR) and the corresponding dynamic constraint coefficient pruning (DCCP) computation method, which fully consider the volt/var characteristics of bulk power systems, are proposed in this letter. Both linearized and nonlinearized robust optimization problems are introduced to obtain accurate results. The computational accuracy, time cost, and advantages of autonomous-synergic control are observed in the simulation results.**

***Index Terms*—Voltage security region, cascading failure, dynamic constraint coefficient pruning (DCCP), bulk power system, robust optimization.**

I. Introduction

BULK power systems exhibit volt/var control deterioration, particularly in scenarios with heavy loads or high penetration level of renewable energies, resulting in large-scale cascading tripping failures [1], [2]. This poses one of the major challenges of bulk power systems. For example, in January, 2014 in the Gansu Power Grid in western China, the direct current (DC) -blocking contingency triggered by a three-phase grounded fault caused a 0.2 p.u. voltage increase in the high-voltage direct current (HVDC) converter station, resulting in large-scale tripping of renewable power generation by high-voltage protection systems.

An effective means of voltage control to prevent large-scale cascading failures using a stepwise search method is to determine certain security voltage control ranges for all stations [1], [3]. This primarily deals with large-scale issues in wind power integration areas [4]. Voltage security regions in power injection spaces for distribution power systems, which can significantly simplify the solution to the optimization problem, were introduced in [5]. In the last few decades, data and information communication applications have achieved tremendous progress and have become a major foundation for future smart grids [6]. However, certain challenges remain.

First, insufficient dynamic reactive power reserves or conventional power plants, weak network connections, and limited voltage/var control capabilities still exist in current power systems. It is generally difficult to maintain a constant voltage when the demand varies in scenarios with heavy loads or high penetration level of renewable energies. Therefore, compared with the decoupled voltage control scheme, the autonomous-synergic control is more suitable for current systems. If the voltages of all substations are controlled autonomously, the reactive power control capacities will be extremely restricted. The situation is even worse if the stations do not have sufficient reactive power sources, thus exhibiting conservative feasible ranges of voltage control [7]. By contrast, if the voltages of all substations are controlled in a synergistic manner, the system will not have sufficient time to communicate in online applications [8].

Second, the security region for large-scale systems is a highly nonlinear dimensional space that includes discrete variables and differential algebraic constraints. It is also a challenging issue to determine the security region for online applications, i. e., the accurate and efficient resolution of large-scale, nonlinear, mixed-integer robust optimization problems.

Therefore, to address these challenges, the concept of an autonomous-synergic voltage security region (AS-VSR) is proposed in this letter to prevent cascading failures in bulk power systems. The main contributions of this letter are summarized as follows.

1) The proposed AS-VSR method fully uses the volt/var characteristics of bulk power systems, thereby optimally approximating the volt/var control using fewer hyperplanes. It also overcomes any conservative issues and fully utilizes the voltage-secure operational space.

2) A corresponding dynamic constraint coefficient pruning (DCCP) algorithm is proposed to increase the computational speed, which can be computed only by solving the linear-

Manuscript received: August 9, 2021; revised: October 18, 2021; accepted: January 14, 2022. Date of CrossCheck: January 14, 2022. Date of online publication: February 22, 2022.

This work was supported in part by the National Natural Science Foundation of China (No. 52007017) and Fundamental Research Funds for the Central Universities (No. 2020CDJQY-A027).

F. Li, T. Niu (corresponding author), and L. Xue are with the State Key Laboratory of Power Transmission Equipment & System Security and New Technology, Chongqing University, Chongqing 400044, China (e-mail: 2827417795@qq.com; niutthu@qq.com; 598525139@qq.com).

Y. Li is with Zhejiang University, Hangzhou 310058, China (e-mail: 1319101@zju.edu.cn).

T. Huang and Z. Wu are with the State Grid Hangzhou Power Supply Company, Hangzhou 310020, China (e-mail: huangte1992@foxmail. com; qinshuang@kemov.com).

DOI: 10.35833/MPCE.2021.000550

ized problem to obtain accurate results, thus realizing real-time calculations while guaranteeing accuracy.

II. Concept and Computational Approach of AS-VSR

A. Definition and Mathematical Model of AS-VSR

Constraint (1) represents the general physical operational constraints of power systems in a compact form under normal ($N-0$) conditions and in different $N-1$ scenarios.

$$\begin{cases} \dot{\boldsymbol{x}} = \boldsymbol{f}^s\left(\boldsymbol{x}^s, \boldsymbol{y}^s, \boldsymbol{u}, \boldsymbol{w}\right) \\ \boldsymbol{g}^s\left(\boldsymbol{x}^s, \boldsymbol{y}^s, \boldsymbol{u}, \boldsymbol{w}\right) \geq \boldsymbol{0} \end{cases} \tag{1}$$

where $\boldsymbol{f}(\cdot)$ denotes differential equations that describe system dynamics; $\boldsymbol{g}(\cdot)$ denotes equality and inequality constraints; s denotes the variables in the s^{th} $N-1$ scenario; $\boldsymbol{x}$ is the vector of bus voltage; $\boldsymbol{y}$ is the vector of other state variables; $\boldsymbol{u}$ is the vector of control variables of the var control devices; and $\boldsymbol{w}$ is the vector of system uncertainties such as the active power fluctuations in the renewable energy resources and power system loads. These vectors are confined to certain feasible region spaces defined as:

$$\Omega_{\boldsymbol{u}} := \left\{ \boldsymbol{u} \in \mathbf{R}^{n+1} \,\middle|\, \underline{u}_i \leq u_i \leq \overline{u}_i, i = 1, 2, ..., n+1 \right\} \tag{2}$$

$$\Omega_{\boldsymbol{w}} := \left\{ \boldsymbol{w} \in \mathbf{R}^{r} \,\middle|\, \| \boldsymbol{c}\boldsymbol{w} + \boldsymbol{d} \|_{\infty} \leq 1 \right\} \tag{3}$$

$$\Omega_{\boldsymbol{x}^0} := \left\{ \boldsymbol{x}^0 \in \mathbf{R}^{n+1} \,\middle|\, \exists \boldsymbol{u} \in \Omega_{\boldsymbol{u}}, \forall \boldsymbol{w} \in \Omega_{\boldsymbol{w}}, \boldsymbol{x}^0 \text{ satisfies (1)} \right\} \tag{4}$$

where $\Omega_{\boldsymbol{u}}$ is the feasible region of control variables; u_i is the control variable of the i^{th} var control device; $\underline{u}_i$ and $\overline{u}_i$ are the minimum and maximum limits of control variables of the i^{th} var control device, respectively; $\Omega_{\boldsymbol{w}}$ is the variation range of uncertainty; $\boldsymbol{c}$ and $\boldsymbol{d}$ are the coefficients of uncertainty; $\Omega_{\boldsymbol{x}^0}$ is the feasible region of bus voltage; $\boldsymbol{x}^0$ is the bus voltage under normal operating conditions; and $n+1$ and r are the dimensions of vectors $\boldsymbol{u}$ and $\boldsymbol{w}$, respectively.

The practical VSR of the pilot buses should be the intersection of certain voltage limits and should satisfy all operational constraints, as expressed in (5) and shown in Fig. 1, where $\boldsymbol{x}_P$ is the vector of voltages of pilot buses; $\boldsymbol{x}_{P,\min}$ and $\boldsymbol{x}_{P,\max}$ are the controllable voltage ranges of pilot bus in $N-0$ and $N-1$ scenarios, respectively; and $\underline{\boldsymbol{x}}_P$ and $\overline{\boldsymbol{x}}_P$ are the original voltage ranges of pilot bus.

$$\left[\boldsymbol{x}_{P,\min}, \boldsymbol{x}_{P,\max}\right] = \left[\underline{\boldsymbol{x}}_P, \overline{\boldsymbol{x}}_P\right] \cap \left\{ \boldsymbol{x}_P \,\middle|\, \boldsymbol{x}_P \in \Omega_{\boldsymbol{x}^0} \right\} \tag{5}$$

The definition of AS-VSR is as follows: if the voltage of the pilot bus is controlled within a certain range, the voltage of the other buses can be independently controlled within their own ranges around the pilot bus without considering the operational details of the other buses/stations. For example, as shown in Fig. 1(c), the pilot and other buses can control their voltages within $\left[\boldsymbol{x}_{P,\min}, \boldsymbol{x}_{P,\max}\right]$ and $\left[\boldsymbol{x}'_{i,\min}, \boldsymbol{x}'_{i,\max}\right]$ in a decoupled manner. As the volt/var feasible region is always hyperquadrangular in the voltage operational space, AS-VSR provides a promising and practical method for large-scale automatic voltage control (AVC) systems. It should be noted that the AS-VSR proposed in this letter is determined in the voltage operational state space. For operators, it is sometimes critical to determine certain voltage control ranges, particularly for pilot buses in power systems. In these situations, operators can monitor the voltage security of power system by determining whether the voltages of the pilot buses are located in their own security regions. The red and green regions in Fig. 1 represent the autonomous voltage security region (A-VSR) [7], [8] and AS-VSR in the power systems, respectively, where the AS-VSR uses a more feasible voltage operational space compared with the A-VSR.

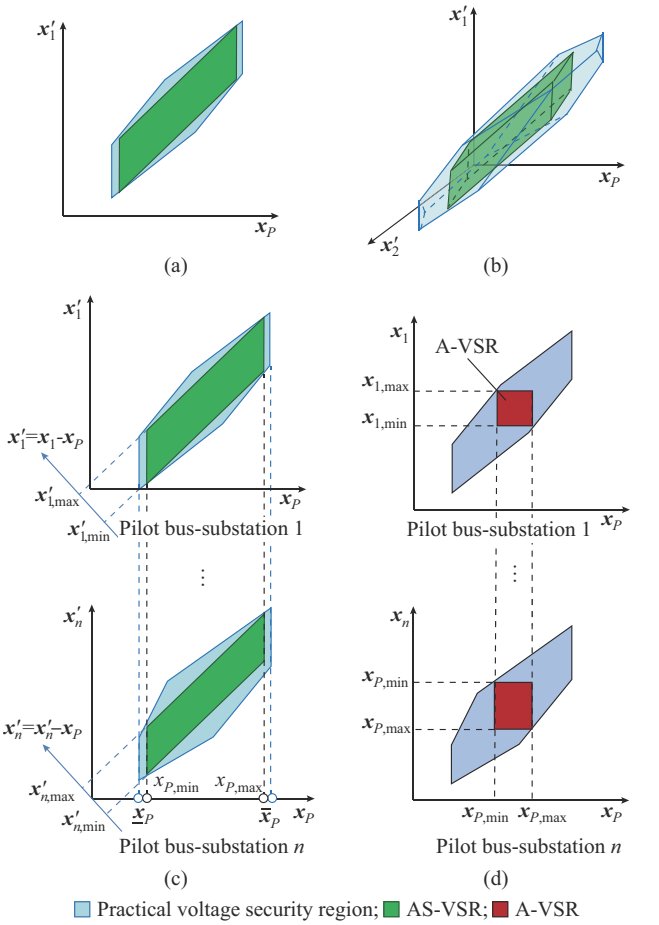

Fig. 1. AS-VSR in voltage operational space of different dimensions. (a) 2-dimensional. (b) 3-dimensional. (c) $(n+1)$-dimensional. (d) Comparison of A-VSR.

To formulate the mathematical model of the AS-VSR, the $(n+1)$-dimensional voltage vector $\boldsymbol{x}$ is reordered as $\boldsymbol{x} = \left[\boldsymbol{x}_P, x_1, x_2, \ldots, x_n\right]^{\mathrm{T}}$, where the subscript P denotes the pilot bus. For convenience, a mapping function $f: \mathbf{R}^{n+1} \rightarrow \mathbf{R}^{n+1}$ is defined in (6) to describe the AS-VSR. The AS-VSRs in 2-, 3-, and $(n+1)$-dimensional spaces are depicted in Fig. 1(a), 1(b), and (c), respectively. In different dimensional spaces, according to the definition of the AS-VSR, the different 2-dimensional projections of the AS-VSR are also quadrangular. It should be noted that in field applications, power system operators often choose buses with higher voltage levels, relatively higher short-circuit ratios, large power plant capacity allocations, or heavy system loads as pilot buses. Usually,

pilot buses are critical system generators, loads, and substations that allocate a large capacity of reactive power devices. It is essential to maintain and control the voltages of these pilot buses within their security regions. One purpose in this letter is to construct a maximal hyperquadrangular to determine the VSRs, of which the hyperplanes can be used in optimization problems as security constraints, thus decreasing the problem scales and saving computational time.

$$\boldsymbol{x}'=f(\boldsymbol{x}):=\boldsymbol{x}-\boldsymbol{x}_P\begin{bmatrix}0 & \boldsymbol{1}_{1\times n}\end{bmatrix}^{\mathrm{T}} \tag{6}$$

Finally, the AS-VSR can be formulated as an optimization problem expressed by (7) and (8) that aim to obtain the largest inner hyperparallelograms (7) in the feasible regions (8) while considering system uncertainties.

$$\max_{\boldsymbol{u}} \left\| \boldsymbol{\lambda}^{\mathrm{T}}\left(\boldsymbol{x}'^{0}_{\max}-\boldsymbol{x}'^{0}_{\min}\right)\right\| \tag{7}$$

s.t.

$$\boldsymbol{x}'^{0}\in\Omega_{\boldsymbol{x}'^{0}} \quad \forall x'^{0}_{i}\in\left[\boldsymbol{x}'^{0}_{\min},\boldsymbol{x}'^{0}_{\max}\right],\forall \boldsymbol{w}\in\Omega_{\boldsymbol{w}} \tag{8}$$

where $\boldsymbol{\lambda}$ is the weight matrix provided by system operators; $\boldsymbol{x}'^{0}$ is voltage amplitude of AS-VSR; and $\boldsymbol{x}'^{0}_{\max}$ and $\boldsymbol{x}'^{0}_{\min}$ are the maximum and minimum voltage amplitudes of AS-VSR, respectively.

However, (7) and (8) cannot be directly solved, particularly for large-scale systems, because of online application demands. Thus, an efficient approach for obtaining an accurate AS-VSR result is introduced in Sections II-B and II-C.

B. Linear Optimization Problem of AS-VSR

If the constraints in (7) and (8) are all linear, an equivalent optimization model can be derived (as shown in the Appendix A) as (9) and (10).

$$\max_{\boldsymbol{u}} \left\| \boldsymbol{\lambda}^{\mathrm{T}}\left(\boldsymbol{x}'^{0}_{\max}-\boldsymbol{x}'^{0}_{\min}\right)\right\| \tag{9}$$

s.t.

$$\boldsymbol{g}^{s,cur}+\left[\boldsymbol{s}_{\boldsymbol{g}^{s}\boldsymbol{u}}\boldsymbol{K}^{-1}\right]^{+}\left(\boldsymbol{x}'^{0}_{\min}-\boldsymbol{x}'^{0,cur}\right)+\left[\boldsymbol{s}_{\boldsymbol{g}^{s}\boldsymbol{u}}\boldsymbol{K}^{-1}\right]^{-}\left(\boldsymbol{x}'^{0}_{\max}-\boldsymbol{x}'^{0,cur}\right)+\left[\boldsymbol{s}_{\boldsymbol{g}^{s}\boldsymbol{w}}\boldsymbol{c}^{-1}\right]^{-}-\left[\boldsymbol{s}_{\boldsymbol{g}^{s}\boldsymbol{w}}\boldsymbol{c}^{-1}\right]^{+}\geq\boldsymbol{0} \quad s=0,1,...,n_s,\boldsymbol{K}=\left[\boldsymbol{s}_{\boldsymbol{z}'^{0}\boldsymbol{u}}\right]_{1:(n+1)} \tag{10}$$

where $[\boldsymbol{A}]^{+}=\max\{\boldsymbol{A},\boldsymbol{0}\}$ and $[\boldsymbol{A}]^{-}=\min\{\boldsymbol{A},\boldsymbol{0}\}$ denote the positive and negative matrices of $\boldsymbol{A}$, respectively; $[\boldsymbol{A}]_{1:n}$ denotes the matrix consisting of the first n^{th} row of matrix $\boldsymbol{A}$; superscript *cur* denotes the current value; matrix $\boldsymbol{s}_{\boldsymbol{xu}}$ is adopted to define the partial differentiation $\boldsymbol{s}_{\boldsymbol{xu}}\equiv\partial\boldsymbol{x}/\partial\boldsymbol{u}$; and n_s is the number of faults set by the system.

C. Nonlinear Optimization Problem of AS-VSR

Based on the linearized problem, the DCCP method is introduced to obtain accurate computational results and reduce the number of linearization errors. Accurate AS-VSR results for nonlinear problem (7) and (8) can be obtained by solving linearized problem (9) and (10) several times with modified coefficients using the DCCP method in each iteration step.

For convenience, the i^{th} vertex $\boldsymbol{v}_i$ of the hyper-quadrangular AS-VSR is defined as (11), and a vertex set Ω_{act} is defined to represent the active vertex, i.e., the elements in the set hold constraint (12) with the physical meaning of locating the vertex outside the feasible region. The superscript denotes the variable values or sets in the corresponding iteration step and 0 represents the initial state.

$$\begin{cases}\boldsymbol{v}_i=\begin{bmatrix}\boldsymbol{x}'^{0}_{\min} & \boldsymbol{x}'^{0}_{\max}\\ \underline{\boldsymbol{w}} & \overline{\boldsymbol{w}}\end{bmatrix}\begin{bmatrix}1\\0\end{bmatrix}+\boldsymbol{a}_i\otimes\left(\begin{bmatrix}\boldsymbol{x}'^{0}_{\min} & \boldsymbol{x}'^{0}_{\max}\\ \underline{\boldsymbol{w}} & \overline{\boldsymbol{w}}\end{bmatrix}\begin{bmatrix}-1\\1\end{bmatrix}\right)\\ \boldsymbol{a}_i\in\mathbf{R}^{n+r+1}\\ a_{ij}\in\{0,1\}\quad \forall j=1,2,...,n+r+1\end{cases} \tag{11}$$

$$\Omega^{(0)}_{act}\triangleq\left\{\boldsymbol{v}^{(0)}_i\,\middle|\,\min_j \boldsymbol{g}_j\left(\boldsymbol{v}^{(0)}_i\right)\leq 0, i\in\{1,2,...,2n+2\}\right\} \tag{12}$$

Following the linearization, the DCCP method uses a known active vertex as the starting vertex. Then, the constraint acting at this vertex is considered as the equality constraint to maximize the objective function (7), and the other constraints remain unchanged for the moment. This process is repeated until the convergence condition is satisfied. The detailed processes of the DCCP method are as follows.

1) Process 1: set the step index $k\rightarrow 0$ and $\Omega^{(k)}_{act}\rightarrow\varnothing$.

2) Process 2: while $k<k_{\max}$, solve linearized problem (9) and (10). In this process, the approximate largest inner hyperparallelograms in the feasible regions can be obtained. Next, we determine whether the vertex obtained by Process 2 belongs to Ω_{act} according to (11).

3) Process 3: solve the nonlinear problem. If the new vertex satisfies (12), update the active set $\Omega^{(k)}_{act}\rightarrow\Omega^{(k)}_{act}\cup\boldsymbol{v}^{(k)}_i$. Then, the constraints acting on this vector are considered as equality constraints, and the other constraints remain unchanged.

4) Process 4: modify and update coefficients.

$$\begin{cases}\left[\boldsymbol{s}_{\boldsymbol{g}^{s}\boldsymbol{u}}\boldsymbol{K}^{-1}\right]^{*}_{pq}\rightarrow\left[\boldsymbol{s}_{\boldsymbol{g}^{s}\boldsymbol{u}}\boldsymbol{K}^{-1}\right]_{pq}sig'\left(\boldsymbol{\Lambda}_p\right)\\ sig'\left(\boldsymbol{\Lambda}_p\right)=1+sig\left(2\boldsymbol{\Lambda}_p-\min_{m\in\{m|\boldsymbol{\Lambda}_m>\boldsymbol{0}\}}\boldsymbol{\Lambda}_m\right)\dfrac{\left[\boldsymbol{v}^{(k)}_i\right]_q-v^{0,cur}_q}{\left[\boldsymbol{g}\left(\boldsymbol{v}^{(k)}_i\right)\right]_q-v^{0,cur}_q}\end{cases} \tag{13}$$

where p and q denote the p^{th} row and q^{th} column of the matrix, respectively; and $\boldsymbol{\Lambda}_p$ is the Lagrange multiplier of the p^{th} constraint in (9) and (10); m is the number of state variables; $v^{0,cur}_q$ is the current vertex of the hyper-quadrangular AS-VSR; $sig(\cdot)$ is the signal function; and $sig'(\cdot)$ is the derivative of the signal function.

To obtain accurate computational results of AS-VSR, (13) is used to determine the pruning coefficient for the linearized problem. It should be noted that the active vertices are still located on the boundary of the nonlinear feasible region after the coefficients are modified, which is a strictly accurate optimal solution for the original nonlinear problem (as shown in Appendix A).

5) Process 5: $k=k+1$ and repeat Processes 2-4 until the convergence conditions in (14) are satisfied.

$$\begin{cases}\dot{\boldsymbol{x}}=\boldsymbol{f}^{s}\left(\boldsymbol{v}^{(k)}_i\right)\\ \left\|\boldsymbol{g}\left(\boldsymbol{v}^{(k)}_j\right)\right\|_{\infty}<\varepsilon\end{cases}\quad\forall\boldsymbol{v}^{(k)}_i\in\Omega^{(k)}_{act},\forall j\in\{1,2,...,2n+2\} \tag{14}$$

Figure 2 shows the computational process of the AS-VSR using the DCCP algorithm in a two-dimensional projection space. In each iteration step, the irregular elliptical-shaped re-

gion represents the nonlinear feasible region, and the region surrounded by black straight lines denotes the linearized region considering (9) and (10). For example, in the first iteration process shown in Fig. 2, following the linearization solution (*Step 3*), the physical operational constraints are assessed using (14), and vertices B and C belong to Ω_{act} (*Step 4*). Then, the coefficients of the linearized problem are modified by the rules of (13), but the convergence condition in (14) does not hold (*Step 5*). This must be determined in a new iteration step by first solving the linearization problem (*Step 6*). Following several iterations, the computation ends and accurate results are finally obtained.

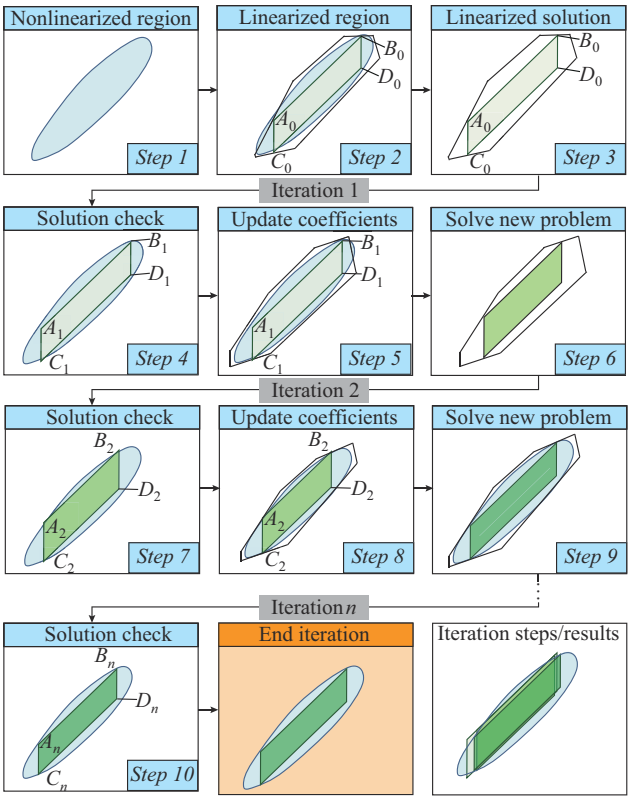

Fig. 2. Computational process of AS-VSR using DCCP algorithm in a two-dimensional projection space.

III. Case Study

Three systems (i.e., IEEE 118-bus, IEEE 300-bus, and IEEE 2383-bus systems) were used in this letter to demonstrate the properties of the proposed AS-VSR. All systems were tested using a laptop computer (processor: Intel Core i5-3230M; CPU: 2.60 GHz; RAM: 8 GB).

First, 2000 operational points were generated around the current operational state. Then, different $N-1$ contingencies were simulated for all operational points, where the secure points were plotted in green in the voltage operational space or in red otherwise. The $N-0$ condition is the base condition of the power system without any contingencies. Regarding the $N-1$ contingencies, they are usually derived from the short circuit of the pilot bus and tripping faults of the transmission lines. In field applications as well as in this letter, different $N-1$ contingencies were selected by contingency screening using a large amount of historical data. This letter used the 30% most severe $N-1$ contingencies as the contingency set. For an operational point, if the system not only operated normally under the $N-0$ conditions but also after any $N-1$ contingencies, it was identified with secure operating points (green). In other words, all the operational limits held under $N-0$ conditions and after all $N-1$ contingencies, including the terminal voltage constraints of substations and the capacity constraints of each transmission line. By contrast, after an $N-1$ contingency, if any operational limit was violated (its upper or lower bound was exceeded), it was identified as having insecure operational points (red). Different two-dimensional projections of the AS-VSR are shown in Fig. 3. Three characteristics and advantages of the AS-VSR could then be obtained.

1) Advantages of autonomous-synergic voltage control: it can be observed from Fig. 3 that the proposed method can guarantee the feasibility of the AS-VSR and parallelogram located in green. As Fig. 3 shows, the real voltage security region is similarly quadrilaterally shaped. Thus, the AS-VSR represents one of the optimal VSR approximations using relatively fewer hyperplanes.

2) Computational accuracy: the vertices of the AS-VSR are near the secure boundary. Some insecure red points are near but outside the AS-VSR. In fact, if the convergence threshold is set at a lower value, the computational result will be more accurate. It should also be noted that insecure red points exist outside the VSR. In other words, there is at least one scenario in which some physical operational constraints cannot hold, which may further cause large-scale cascading failures. In these situations, if an $N-1$ contingency occurs in the power system, the physical operational constraints are violated, and the secure operations of the power system cannot be 100% guaranteed. Thus, it may result in a risk of voltage insecurity.

3) Computational effectiveness: it can be observed from Table I that the computational time increases approximately linearly with the system scale. Regarding large-scale systems, the computation requires approximately 8-12 iteration steps to reach convergence. In real regional systems, the volt/var control/dispatch time interval is usually set at the 5- or 15-min min level. Thus, this method meets the requirements of real applications.

In addition, the voltage security regions in previous studies were compared based on the following aspects.

1) Definition space: [3], [5], [7] are defined in the power injection space to determine the power outputs of each node, whereas [1], [2], [8], and the proposed methods are defined in the voltage operational state space to determine the voltage secure operational range for each bus.

2) Uncertainties: [1]-[3] and the proposed method consider system uncertainties, whereas [5], [7], [8] do not.

3) Conservative issues: [7] and [8] suffer from conservative issues when hypercubes are constructed to determine VSRs, whereas the proposed method fully considers the volt/var control characteristics and constructs hyperquadrangulars to determine VSRs.

4) Independent/decoupled voltage control: [3], [7], [8], and the proposed method can achieve independent voltage control, whereas other studies do not mention this issue.

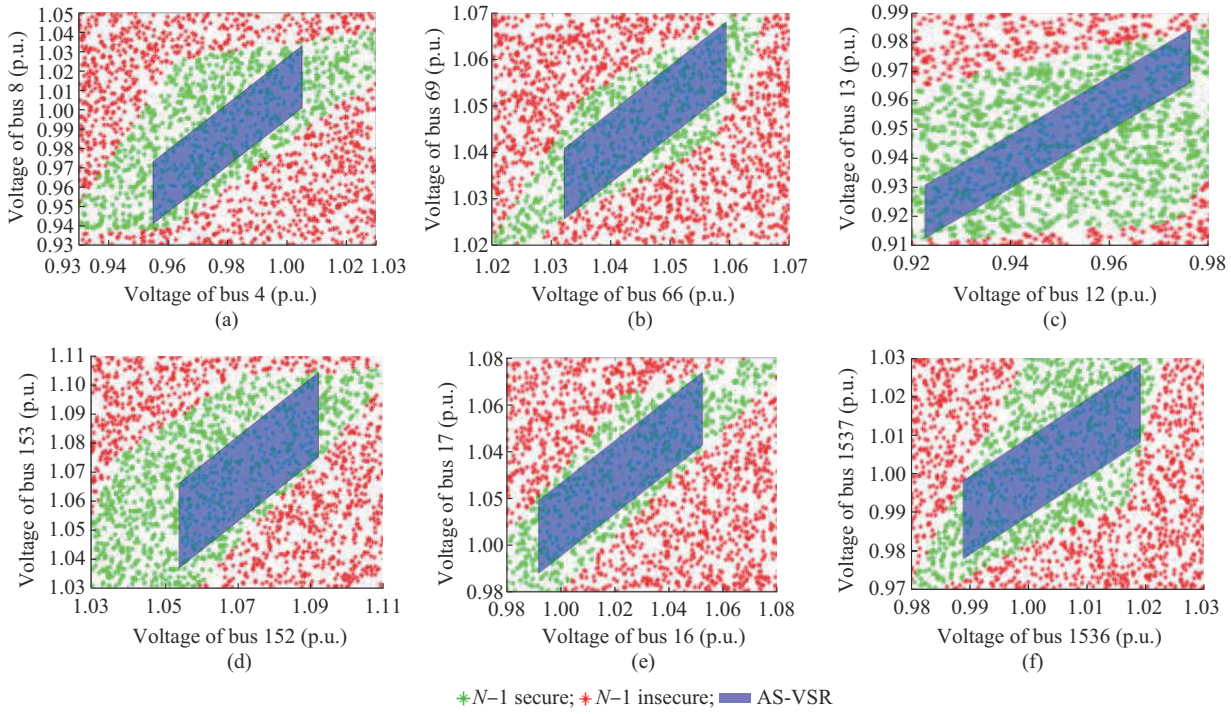

Fig. 3. Different two-dimensional projections of AS-VSR. (a) AS-VSR between bus 4 and bus 8 in IEEE 118-bus system. (b) AS-VSR between bus 66 and bus 69 in IEEE 118-bus system. (c) AS-VSR between bus 12 and bus 13 in IEEE 300-bus system. (d) AS-VSR between bus 152 and bus 153 in IEEE 300-bus system. (e) AS-VSR between bus 16 and bus 17 in IEEE 2383-bus system. (f) AS-VSR between bus 1536 and bus 1537 in IEEE 2383-bus system.

TABLE I
COMPUTATIONAL EFFECTIVENESS OF DIFFERENT IEEE SYSTEMS

System	Iteration step	Computational time (s)				Computational error (%)
		Average linearized model	Model linearization	Time domain simulation	Total	
IEEE 118-bus	5	0.54	0.01	0.69	6.20	0.72
IEEE 300-bus	6	1.57	0.03	1.80	20.40	0.59
IEEE 2383-bus	9	7.10	0.15	6.28	121.77	0.84

5) System dynamics: [5] and the proposed method consider system dynamics, whereas others do not.

IV. CONCLUSION

This letter introduced and proposed the concept of AS-VSR and the corresponding DCCP computational method, which can be used to overcome previous computational burden and conservative issues. The main characteristics and advantages of the AS-VSR, including volt/var control independence, computational speed, and accuracy, were illustrated and verified through analysis of three systems. The proposed method presents guidelines for constructing the largest inner hyperparallelograms in the feasible region and provides an opportunity for conveniently applying them to nonlinear highly dimensional bulk power systems.

APPENDIX A

The equivalent linear optimization model described in Section II is first proven as follows.

A. Proof of Sufficient Condition

When the constraints in (1) are all linear, vector $\boldsymbol{z}'$ is defined as $\boldsymbol{z}'=[\boldsymbol{x}';\boldsymbol{y}]\in\mathbf{R}^{n+m+1}$. When (1) and (6) are differentiated, the partial differentiation $\boldsymbol{s}_{z'^0\boldsymbol{u}}$ between control variable $\boldsymbol{u}$ and state variable $\boldsymbol{z}'^0$ can be derived as (A1).

$$\boldsymbol{s}_{z'^0\boldsymbol{u}}=\begin{bmatrix}-1 & \mathbf{0} & 0\\ \mathbf{1}_{n\times 1} & -\boldsymbol{I}_n & \mathbf{0}\\ 0 & \mathbf{0} & -\boldsymbol{I}_m\end{bmatrix}\boldsymbol{s}_{f^0z^0}^{-1}\boldsymbol{s}_{f^0\boldsymbol{u}} \tag{A1}$$

Considering the linear constraint hypothesis, the explicit function determined in (1) can be described by (A2) for the i^{th} control variable u_i. For convenience, $\boldsymbol{A}_{ij}$ denotes the entry in the i^{th} row and j^{th} column of the matrix $\boldsymbol{A}$.

$$u_i=u_i^{cur}+\sum_{j=1}^{n+1}\left[\boldsymbol{s}_{g^0\boldsymbol{u}}^{-1}\right]_{ij}\left(x'^0_j-x'^{0,cur}_j\right)+\sum_{j=1}^{l}\left[\boldsymbol{K}^{-1}\boldsymbol{s}_{x^{r0}\boldsymbol{w}}\right]_{ij}w_j \tag{A2}$$

In general, the number of uncertainty-related constraints k of a power system described in (3) is less than the dimension of $\Omega_{\boldsymbol{w}}(r)$. These two conditions are described as follows.

1) $k=r$. The invertible mapping of $g:\mathbf{R}^r\to\mathbf{R}^r$ can be defined using (A3):

$$\boldsymbol{w}=g(\boldsymbol{w}')\equiv\boldsymbol{c}^{-1}\boldsymbol{w}'-\boldsymbol{c}^{-1}\boldsymbol{d} \tag{A3}$$

2) $k<r$. The subspace generated by the row vector of matrix $\boldsymbol{c}$ is denoted by (A4). Obviously, a complementary space $\boldsymbol{W}_c'$ can be constructed that satisfies (A5).

$$\boldsymbol{W}_c = span\left(\boldsymbol{c}_1, \boldsymbol{c}_2, ..., \boldsymbol{c}_k\right) \tag{A4}$$

$$\begin{cases} \boldsymbol{W}_c' = span\left(\boldsymbol{c}_{k+1}, \boldsymbol{c}_{k+2}, ..., \boldsymbol{c}_r\right) \\ \dim\left(\boldsymbol{W}_c'\right) = r-k \\ \dim\left(\boldsymbol{W}_c \oplus \boldsymbol{W}_c'\right) = r \end{cases} \tag{A5}$$

where *span*(·) donates the span of vectors $(\boldsymbol{c}_1, \boldsymbol{c}_2, ..., \boldsymbol{c}_k)$; and dim(·) represents the dimension of vectors.

Thus, the general matrices $\boldsymbol{c}$ and $\boldsymbol{d}$ can be constructed as expressed in (A6), which also satisfies the mapping defined in (A3). Here, $\boldsymbol{M}$ denotes a matrix with a relatively large positive number for each entry:

$$\begin{cases} \boldsymbol{c} = \left[\, \boldsymbol{c}_1^{\mathrm{T}} \;\; \boldsymbol{c}_2^{\mathrm{T}} \;\; ... \;\; \boldsymbol{c}_r^{\mathrm{T}} \,\right]^{\mathrm{T}} \\ \boldsymbol{d} = \left[\, \boldsymbol{1}^{\mathrm{T}} \;\; \boldsymbol{M} \,\right]^{\mathrm{T}} \end{cases} \tag{A6}$$

With $\forall x'^{0}_i \in \left[x^{0}_{i,\min}, x^{0}_{i,\max}\right]$, $\forall \boldsymbol{w} \in \Omega_{\boldsymbol{w}}$, and with the focus on the i^{th} constraint of (10), g_i^s satisfies (A7), and the constraint in (10) holds. It can be similarly proven that constraint (10) holds (i.e., $\boldsymbol{x}'^{0} \in \Omega_{\boldsymbol{x}'^{0}}$); thus, the proof of a sufficient condition is provided.

$$\begin{aligned} g_i^s = g_i^{s,cur} &+ \sum_{j=1}^{n+1}\left[\boldsymbol{s}_{\boldsymbol{g}^s\boldsymbol{u}}\right]_{ij}\left(u_j - u_j^{cur}\right) + \sum_{k=1}^{r}\left[\boldsymbol{s}_{\boldsymbol{g}^s\boldsymbol{w}}\right]_{ik} w_k = g_i^{s,cur} + \\ &\sum_{j=1}^{n+1}\left[\boldsymbol{s}_{\boldsymbol{g}^s\boldsymbol{u}}\right]_{ij}\sum_{k=1}^{n}\boldsymbol{K}_{jk}^{-1}\left(x_j' - x_j'^{cur}\right) + \sum_{j=1}^{r}\left[\boldsymbol{s}_{\boldsymbol{g}^s\boldsymbol{w}}\right]_{ij}\sum_{k=1}^{n}\boldsymbol{c}_{jk}^{-1} w_k' = g_i^{s,cur} + \\ &\sum_{j=1}^{n+1}\left[\boldsymbol{s}_{\boldsymbol{g}^s\boldsymbol{u}}\boldsymbol{K}^{-1}\right]_{ij}\left(x_j' - x_j'^{cur}\right) + \sum_{k=1}^{r}\left[\boldsymbol{s}_{\boldsymbol{g}^s\boldsymbol{w}}\boldsymbol{c}^{-1}\right]_{ik} w_k' \ge g_i^{s,cur} + \\ &\sum_{j=1}^{n+1}\left[\boldsymbol{s}_{\boldsymbol{g}^s\boldsymbol{u}}\boldsymbol{K}^{-1}\right]_{ij}^{-}\left(x'_{\max,j} - x_j'^{cur}\right) + \sum_{j=1}^{n+1}\left[\boldsymbol{s}_{\boldsymbol{g}^s\boldsymbol{u}}\boldsymbol{K}^{-1}\right]_{ij}^{+}\left(x'_{\min,j} - x_j'^{cur}\right) + \\ &\sum_{k=1}^{r}\left[\boldsymbol{s}_{\boldsymbol{g}^s\boldsymbol{w}}\boldsymbol{c}^{-1}\right]_{ik}^{-} - \sum_{k=1}^{r}\left[\boldsymbol{s}_{\boldsymbol{g}^s\boldsymbol{w}}\boldsymbol{c}^{-1}\right]_{ik}^{+} \ge 0 \end{aligned} \tag{A7}$$

B. Proof of Necessary Condition

For entry g_i^s, the corresponding x_j^{0} and w_k' are first constructed as (A8).

$$\begin{cases} x_j^{0} = \left(x_{j,\max}^{0} - x_{j,\min}^{0}\right) sig\left(\left[\boldsymbol{s}_{\boldsymbol{g}^s\boldsymbol{u}}\boldsymbol{K}^{-1}\right]_{ij}\right) + x_{j,\min}^{0} \\ w_k' = 2sig\left(\left[\boldsymbol{s}_{\boldsymbol{g}^0\boldsymbol{w}}\boldsymbol{c}^{-1}\right]_{ik}\right) - 1 \end{cases} \tag{A8}$$

When (A8) is substituted into constraint (8) while considering the linear constraint hypothesis, the expression of the positive value/function $g_i^s\left(x_j^{0}, w_k'\right)$ can be obtained as (A9), thereby proving the necessary condition.

$$\begin{aligned} 0 \le g_i^s = g_i^{s,cur} &+ \sum_{j=1}^{n+1}\left[\boldsymbol{s}_{\boldsymbol{g}^s\boldsymbol{u}}\right]_{ij}\left(u_j - u_j^{cur}\right) + \sum_{k=1}^{r}\left[\boldsymbol{s}_{\boldsymbol{g}^s\boldsymbol{w}}\right]_{ik} w_k = g_i^{s,cur} + \\ &\sum_{j=1}^{n+1}\left[\boldsymbol{s}_{\boldsymbol{g}^s\boldsymbol{u}}\boldsymbol{K}^{-1}\right]_{ij}\left(x_j' - x_j'^{cur}\right) + \sum_{k=1}^{r}\left[\boldsymbol{s}_{\boldsymbol{g}^s\boldsymbol{w}}\boldsymbol{c}^{-1}\right]_{ik} w_k' = g_i^{s,cur} + \\ &\sum_{j=1}^{n+1}\left[\boldsymbol{s}_{\boldsymbol{g}^s\boldsymbol{u}}\boldsymbol{K}^{-1}\right]_{ij}^{-}\left(x'_{\max,j} - x_j'^{cur}\right) + \sum_{j=1}^{n+1}\left[\boldsymbol{s}_{\boldsymbol{g}^s\boldsymbol{u}}\boldsymbol{K}^{-1}\right]_{ij}^{+}\left(x'_{\min,j} - x_j'^{cur}\right) + \\ &\sum_{k=1}^{r}\left[\boldsymbol{s}_{\boldsymbol{g}^s\boldsymbol{w}}\boldsymbol{c}^{-1}\right]_{ik}^{-} - \sum_{k=1}^{r}\left[\boldsymbol{s}_{\boldsymbol{g}^s\boldsymbol{w}}\boldsymbol{c}^{-1}\right]_{ik}^{+} \end{aligned} \tag{A9}$$

This completes the proof of an equivalent linear optimization model.

Second, the pruning coefficient for the linearized problem is proven as follows.

For the optimal solution $\boldsymbol{v}_i^{(k)*}$ of the linearized problem (9) and (10) in the k^{th} iteration obtained by replacing the coefficients according to the rules given in (13), there exist a corresponding positive vector $\boldsymbol{\varepsilon}_v$ and a modified vertex set $\boldsymbol{v}_i^{(k),mod}$ defined by (A10) such that $\left\| \boldsymbol{\varepsilon}_v \right\|_\infty < 1$ and $\boldsymbol{v}_i^{(k),mod}$ are located on the boundary of the nonlinear VSR $\Omega_{\boldsymbol{x}'^{0}}$. In other words, $\boldsymbol{v}_i^{(k),mod}$ is a strictly accurate optimal solution of the original nonlinear problem (7) and (8).

$$\boldsymbol{v}_i^{(k),mod} = \varepsilon_{v,i}\boldsymbol{v}_i^{(k)*} + \left(1 - \varepsilon_{v,i}\right)\boldsymbol{v}_j^{(k)*} \tag{A10}$$

$$\forall \boldsymbol{v}_i^{(k)} \in \Omega_{act}^{(k)} \bigcup \Omega_{iact,n}^{(k)} \tag{A11}$$

$$\Omega_{\boldsymbol{v}} = \Omega_{act}^{(k)} \oplus \Omega_{iact,n}^{(k)} \oplus \Omega_{iact,r}^{(k)} \tag{A12}$$

$$\begin{aligned} \Omega_{iact,n}^{(k)} \triangleq \Bigg\{ \boldsymbol{v}_i^{(k)} \Bigg| &\left\| \boldsymbol{g}\left(\boldsymbol{v}_i^{(k)}\right) \right\|_\infty < 2 \min_{\left\{i \,\middle|\, \min_j \boldsymbol{g}_j\left(\boldsymbol{v}_i^{(k)}\right) < 0\right\}} \left\| \boldsymbol{g}\left(\boldsymbol{v}_i^{(k)}\right) \right\|_\infty, \\ &i \in \left\{1, 2, ..., 2n+2\right\} \Bigg\} \end{aligned} \tag{A13}$$

where $\Omega_{\boldsymbol{v}}$ is the set representing all vertices, which is further decomposed into three subsets given in (A12); and $\Omega_{iact,n}^{(k)}$ and $\Omega_{iact,r}^{(k)}$ denote the inactive-near and remote-boundary vertex sets, with the physical meaning that the inactive vertex is located inside but near or far away from the VSR boundary.

Proof for the coefficient pruning rules given in (8), it can be further concluded through derivation (A14) that vertex $\boldsymbol{v}_i^{(k)*}$ is located on the boundary of nonlinear VSR $\Omega_{\boldsymbol{x}'^{0}}$.

$$\begin{aligned} \left[\boldsymbol{g}\left(\boldsymbol{v}_i^{(k)*}\right)\right]_q &= g_q^{s,cur} + \sum_{j=1}^{n}\left[\boldsymbol{s}_{\boldsymbol{g}^s\boldsymbol{u}}\boldsymbol{K}^{-1}\right]_{qj}^{*}\left(x'^{*}_j - x_j'^{cur}\right) + \\ &\sum_{j=1}^{r}\left[\boldsymbol{s}_{\boldsymbol{g}^s\boldsymbol{w}}\boldsymbol{c}^{-1}\right]_{qj}^{*} w'^{*} = g_q^{s,cur} + \sum_{j=1}^{n}\left[\boldsymbol{s}_{\boldsymbol{g}^s\boldsymbol{u}}\boldsymbol{K}^{-1}\right]_{qj} sig'\left(\Lambda_j\right)\left(x'^{*}_j - x_j'^{cur}\right) + \\ &\sum_{j=1}^{r}\left[\boldsymbol{s}_{\boldsymbol{g}^s\boldsymbol{w}}\boldsymbol{c}^{-1}\right]_{qj} sig'\left(\Lambda_j\right) w'^{*} = g_q^{s,cur} + \sum_{j=1}^{n}\left[\boldsymbol{s}_{\boldsymbol{g}^s\boldsymbol{u}}\boldsymbol{K}^{-1}\right]_{qj}\left(x'^{*}_j - x_j'^{cur}\right) + \\ &\sum_{j=1}^{n}\left[\boldsymbol{s}_{\boldsymbol{g}^s\boldsymbol{u}}\boldsymbol{K}^{-1}\right]_{qj} w' = \left[\boldsymbol{g}\left(\boldsymbol{v}_i^{(k)}\right)\right]_q = 0 \end{aligned} \tag{A14}$$

Clearly, $\boldsymbol{v}_i^{(k)*}$ is a feasible solution to the original nonlinear problem (6). A vector $\boldsymbol{\varepsilon}_v$ is then constructed as (A15).

$$\boldsymbol{\varepsilon}_v = \arg\left(\max_{\left\{\boldsymbol{\varepsilon}_v \,\middle|\, \boldsymbol{g}\left(\varepsilon_{v,i}\boldsymbol{v}_i^{(k)*} + \left(1-\varepsilon_{v,i}\right)\boldsymbol{v}_j^{(k)*}\right) \ge \boldsymbol{0},\ \forall \boldsymbol{v}_i^{(k)*} \in \Omega_{\boldsymbol{v}}, \boldsymbol{v}_j^{(k)*} \in \Omega_{act}^{(k)}\right\}} \prod \varepsilon_{v,i} \right) \tag{A15}$$

This guarantees that $\boldsymbol{v}_i^{(k),mod}$ is also located at the boundary of VSR $\Omega_{\boldsymbol{x}'^{0}}$. Based on (A15), it can be concluded that $\boldsymbol{v}_i^{(k),mod}$ is a strictly accurate optimal solution to the original nonlinear problem (7) and (8).

It should be noted that the unusual condition with a relatively lower probability that sometimes occurs when resolving volt/var-related OPF problems is $\Omega_{act}^{(0)} = \varnothing$. However, (14) does not hold, with the physical meaning that all vertices of the optimal solution of the original linear problem (9) and (10) are lo-

cated within the VSR boundary. Under this condition, a corresponding value ε_v' and vertex $\boldsymbol{v}_i'^{(k)}$ can first be constructed using (A16) such that $\boldsymbol{v}_i'^{(k)}$ is located on the boundary of the VSR.

$$\begin{cases} \varepsilon_v' = \arg\left(\max_{\left\{\varepsilon_v' \middle| \boldsymbol{g}\left(\boldsymbol{v}_i'^{(k)}\right) \geq \boldsymbol{0}\right\}} \varepsilon_v' \right) \\ \boldsymbol{v}_i'^{(k)} = \left(1-\varepsilon'\right)\boldsymbol{v}_i'^{(k),cen} + \varepsilon_v' \boldsymbol{v}_i'^{(k)} \end{cases} \tag{A16}$$

where $\boldsymbol{v}_i'^{(k),cen}$ denotes the center of the cube surrounded by the vertex $\boldsymbol{v}_i'^{(k)}$. Therefore, the modified vertex $\boldsymbol{v}_i^{(k),mod}$ can be similarly constructed using (A13), which is also a strictly accurate optimal solution to the original nonlinear problem (7) and (8).

This completes the proof.

REFERENCES

[1] Q. Guo, H. Sun, B. Wang *et al.*, "Hierarchical automatic voltage control for integration of large-scale wind power: design and implementation," *Electric Power Systems Research*, vol. 120, pp. 234-241, Mar. 2015.

[2] F. Xu, Q. Guo, H. Sun *et al.*, "A two-level hierarchical discrete-device control method for power networks with integrated wind farms," *Journal of Modern Power Systems and Clean Energy*, vol. 7, no. 1, pp. 88-98, Jan. 2019.

[3] T. Niu, Q. Guo, H. Sun *et al.*, "Autonomous voltage security regions to prevent cascading trip faults in wind turbine generators," *IEEE Transactions on Sustainable Energy*, vol. 7, No. 3, pp. 1306-1316, Jul. 2016.

[4] M. N. Naz, S. Imtiaz, M. K. L. Bhatti *et al.*, "Dynamic stability improvement of decentralized wind farms by effective distribution static compensator," *Journal of Modern Power Systems and Clean Energy*, vol. 9, no. 3, pp. 516-525, May 2021.

[5] T. Yang and Y. Yu, "Static voltage security region-based coordinated voltage control in smart distribution grids," *IEEE Transactions on Smart Grid*, vol. 9, no. 6, pp. 5494-5502, Nov. 2018.

[6] I. Kouveliotis-Lysikatos, N. Hatziargyriou, Y. Liu *et al.*, "Towards an internet-like power grid," *Journal of Modern Power Systems and Clean Energy*, vol. 10, no. 1, pp. 1-11, Jan. 2022.

[7] F. Capitanescu, "Assessing reactive power reserves with respect to operating constraints and voltage stability," *IEEE Transactions on Power Systems*, vol. 26, no. 4, pp. 2224-2234, Nov. 2011.

[8] C. Liu, "A new method for the construction of maximal steady-state security regions of power systems," *IEEE Transactions on Power Systems*, vol. 1, no. 4, pp. 19-26, Nov. 1986.

Fan Li received the B.S. degree from School of Electrical and Power Engineering in China University of Mining and Technology, Xuzhou, China, in 2020. He is currently pursuing the master's degree in Chongqing University, Chongqing, China. His research interests mainly include voltage stability analysis, reliability evaluation, and optimization algorithm.

Tao Niu received the Ph.D. degrees from Tsinghua University, Beijing, China, in 2019. He is currently an Assistant Professor with Chongqing University, Chongqing, China. His research interests include power system transient stability analysis, economic dispatch and control of sending-end and receiving-end, and mathematical model and optimization algorithm in power system.

Lin Xue received the B.S. degree from School of Electrical and Power Engineering of Qinghai University, Xining, China, in 2020. He is currently pursuing his Ph.D. degree in the School of Electrical Engineering of Chongqing University, Chongqing, China. His current research interests include voltage security margin and dynamic var reserve assessment.

Yuxiao Li received the M.D. degree from Peking Union Medical College, Beijing, China, in 2018. Now she is working in the First Affiliated Hospital, College of Medicine, Zhejiang University, Hangzhou, China. Her current research interests include application of big data analysis and calculation method in pharmaceutical industry, and oxidative stress in preeclampsia.

Tianen Huang received the Ph.D. degree from Tsinghua University, Beijing, China, in 2019. Now he is an engineer in the State Grid Hangzhou Power Supply Company, Hangzhou, China. His current research interests include deep learning and artificial neural network and its application in power system.

Zhenjie Wu received the master's degree from North China Electric Power University, Beijing, China, in 2004. He is currently the Director of Electric Power Dispatching Control Center in the State Grid Hangzhou Power Supply Company, Hangzhou, China. His current research interests include power system dispatching, control, and optimization.